Shadow imaging法による（人工）火山灰の形状・動的沈降挙動の精査

服部康男（電中研）
中尾圭佑，須藤仁，竹内晋吾（電中研）

Thanks to 三浦さん，土志田さん，伊藤さん，上澤さん

電力中央研究所

Outline

降下火山灰の気中の運動と形状・姿勢・サイズとの同時把握を可能とする計測システムを検討した.

・シャドーイメージ法により，様々な粒子直径・真球度・沈降速度に対応可能であることを確認した.

・模擬火山灰の沈降挙動を対象に計測を行い，模擬火山灰が，非球形形状と姿勢の多様性とに起因して，沈降速度も多様性を有すること，その沈降速度の絶対値は，比重が半分程度の粒子から同程度の粒子の値に相当すること，を明らかにした.

Tephra fall impacts from the 2011 Shinmoe-dake eruption Japan

Magill C et al. (2013) EPS.

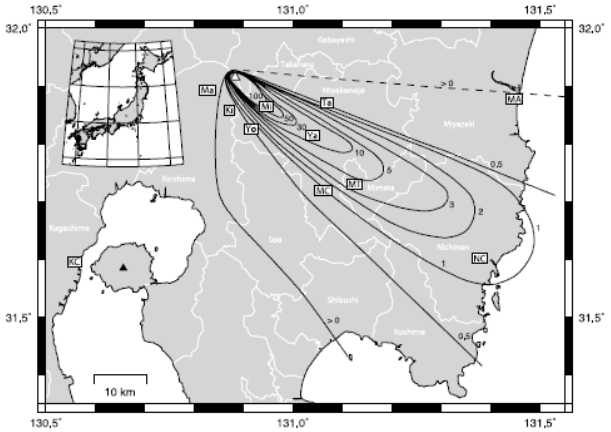

Fig. 1. Area impacted by tephra falls from the 2011 Shinmoedake eruption. Isomass contours are in kg/m^2 and describe tephra accumulation prior to 28th January (AIST, 2011). Municipality boundaries are in white. Letters in boxes refer to place names mentioned in the text: KC Kagoshima City Hall (central Kagoshima), Ki Kirishima, Ma Makizono, MA Miyazaki Airport, MC Miyakonojo City Hall (central Miyakonojo), Mi Miike, MT Mimata Town Hall (central Mimata), NC Nichinan City Hall (central Nichinan), Ta Takazaki, Ya Yamada and Yo Yoshinomoto. White triangle Shinmoedake volcano and black triangle Sakurajima volcano.

Fig. 4. Spinach and cabbage crops in Yamada damaged by tephra (2 February 2011). Photo in top left shows a typical home garden in the area while the other three show rows of vegetables in small farms.

Table 4. Approximate road lengths (km) impacted by various ranges of tephra accumulation (see Fig. 2(b)). Road maps and classifications from OpenStreetMap; isomass contours from AIST (2011).

Tephra accumulation (kg/m^2)	motorway	trunk	primary	secondary	tertiary	urban	rural	all roads
0–0.5	59.7	139.0	238.0	196.3	347.9	1354.9	1342.1	**3678.0**
0.5–1	3.2	65.9	68.2	19.7	63.0	259.5	257.2	**736.9**
1–2	4.7	35.9	87.8	7.7	53.3	119.9	171.6	**480.8**
2–3	6.8	11.6	28.8	9.7	36.2	127.7	157.0	**377.9**
3–5	16.7	12.6	42.3	11.4	59.3	271.5	238.7	**652.5**
5–10	16.1	17.1	21.0	9.8	101.3	170.3	241.8	**577.4**
10–30	9.5	6.2	21.0	10.0	30.6	89.8	149.6	**316.7**
30–50		1.5	1.8	3.7	1.8	15.3	11.5	**35.6**
50–100		3.0	2.0	0.7	0.2	12.2	4.3	**22.3**
>100						2.0		**2.0**
Total	**116.8**	**292.8**	**511.0**	**269.0**	**693.6**	**2423.1**	**2573.8**	**6880.1**

Table 5. Estimated exposure of Kyushu Electric Power Company network to tephra fall; see Fig. 2(b). Approximations of electricity lines given by KEPC and Isomass contours by AIST (2011).

	Approximated length (km)				Facilities affected	
Tephra load (kg/m^2)	500 kV	220 kV	110 kV	60 kV	Hydro stations	Transforming stations
0–0.5	3.4	59.3	28.3	44.6	3	8
0.5–1		5.5	4.4	12.2	1	1
1–2		3.3	1.3	16.2		2
2–3		4.6	1.8	10.9		1
3–5		4.9	2	16.6		1
5–10		5.2	2.4	21.2		2
10–30		5.5	4.3	1.5		1
Total	**3.4**	**88.3**	**44.5**	**123.2**	**4**	**16**

Table 6. Estimated exposure of rail lines and stations to tephra fall; see Fig. 2(c). Lines and stations digitised from Bing aerial imagery and Isomass contours from AIST (2011).

	Kitto line		Nichinan line		Nippo line	
Tephra load (kg/m^2)	Length (km)	Stations	Length (km)	Stations	Length (km)	Stations
0–0.5	6.32	2	41.80	17	48.63	9
0.5–1	0.63	0	20.14	5	6.83	2
1–2	0.42	0	26.37	5	2.66	0
2–3	3.07	0			5.15	1
3–5	4.36	2			5.83	1
5–10	3.69	1			6.22	2
10–30	3.93	1				
Total	**22.42**	**6**	**88.31**	**27**	**75.32**	**15**

Tephra fall impacts to electric power system

Wilson TM et al. (2011) Phys C Earth
Wardman JB et al. (2012) Bull Volcanol

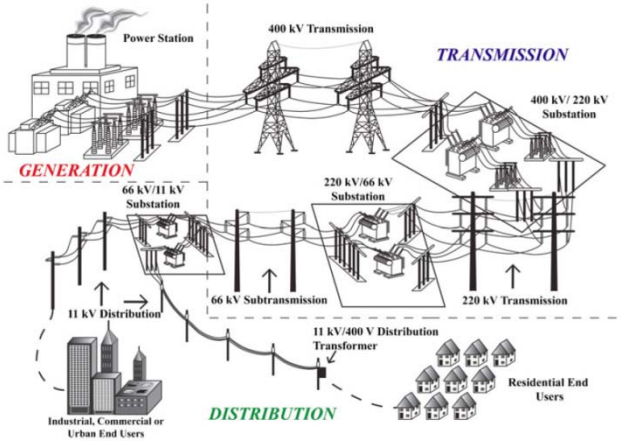

Fig. 2 An example of a modern electric power system. Electric energy is generated at a power station (e.g. 13 kV). From here, the voltage is increased (current decreased) and the energy transmitted at 400 kV via extra-high voltage (EHV) transmission lines to a 400/220 kV EHV substation. The energy is then transmitted to a HV substation where the voltage is reduced to 66 kV. Sub-transmission lines connect the HV substations to many distribution substations located within cities, where the voltage is reduced to 11 kV and the energy finally distributed either directly to industrial plants or factories or to local residential and commercial zones. Distribution transformers (ground or pole mounted) reduce the voltage from 11 kV to ~400/220 V (depending on the system used) for use in homes, shopping centres and other local loads (adapted from Karady 2007)

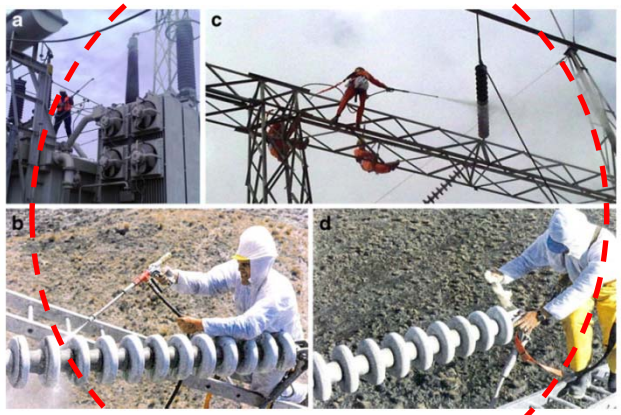

Fig. 5 **a** High-pressure de-energised washing of a power transformer bushing at a sub-station in Ecuador following the 2010 eruption of Tungurahua. **b** A linesman cleans tephra from a de-energised 220 kV strain (horizontally strung) insulator located ~15 km from Ruapehu, New Zealand. **C** Linesmen cleaning de-energised insulators at a Guayaquil, Ecuador sub-station after 1–2 mm of fine-grained tephra fell following the 2010 Tungurahua eruption. **d** Hand-cleaning tephra from a de-energised 220 kV strain in-sulator after the 25 September 1995 Ruapehu eruption. Photo credits: **a** Transelectric, **b** Transpower, **c** Transelectric, **d** Transpower

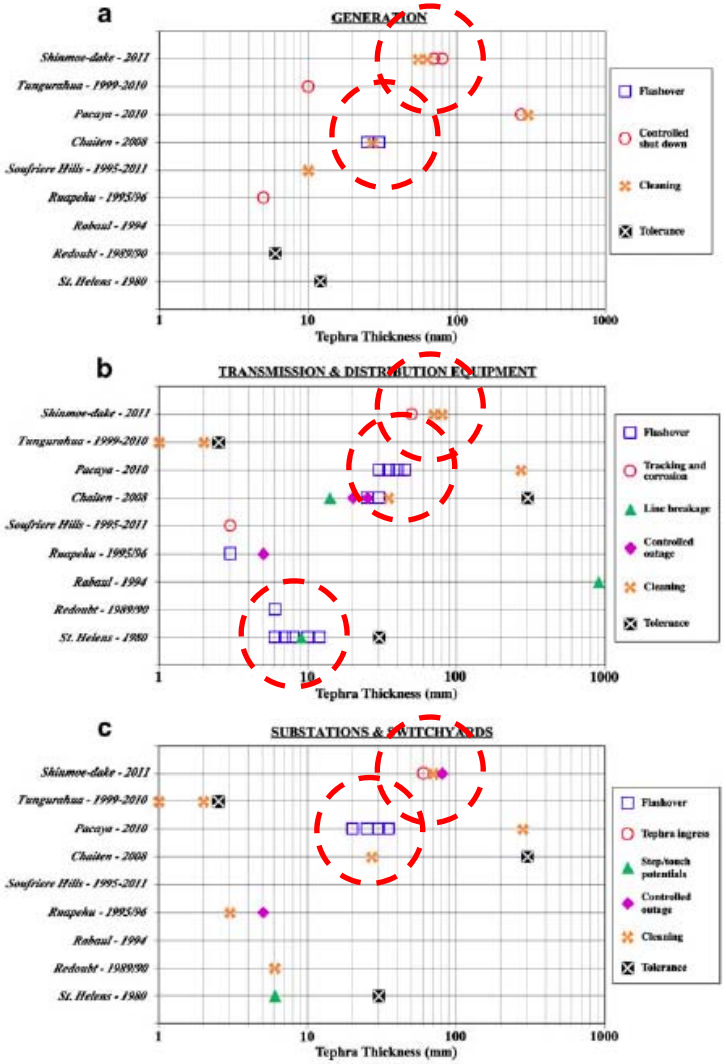

Numerical simulation on tephra fall for Hoei eruption of Fujisan Japan

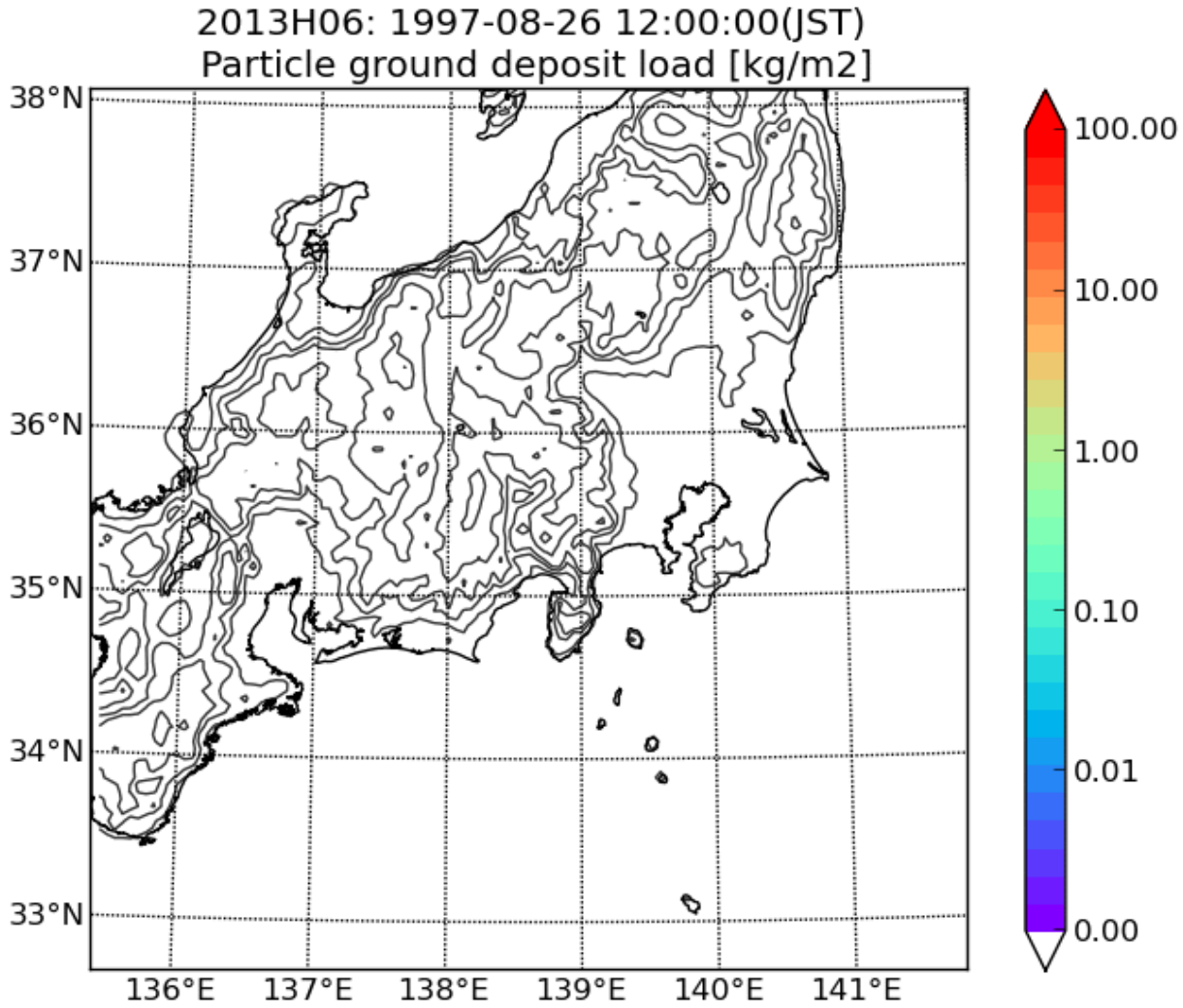

Effect of size, shape and terminal velocity on predicted ground load

Scollo S. et al. (2008) JVGR.

Table 3
Values of Δ for the run sets (Table 2). Comparison is always against the reference run (RUN0). Results for WPS and SPS and for the three models. Green colours indicate low differences $\Delta \leq 0.33$, yellow moderate differences $(0.33 < \Delta \leq 0.66)$, orange high differences $(0.66 < \Delta \leq 0.99)$ and, finally, red extreme differences $(\Delta \geq 1)$

	Weak Plume Scenario (WPS)			Strong Plume Scenario (SPS)		
	FALL3D	HAZMAP	TEPHRA	FALL3D	HAZMAP	TEPHRA
1. Erupted mass						
RUN1-1	1.00	1.00	1.00	1.00	1.00	1.00
2. Topography effects						
RUN2-1	0.11	2.27	1.91	0.21	0.82	0.75
3. Column he ight						
RUN3-1	0.25	0.15	0.13	0.33	0.26	0.17
RUN3-2	0.18	0.13	0.10	0.22	0.19	0.13
4. Column model						
RUN4-1	0.73	0.48	0.32	0.91	0.77	0.45
RUN4-2	0.65	0.22	0.19	1.02	0.50	0.48
RUN4-3	0.81	0.46	0.35	0.84	0.60	0.45
RUN4-4	0.75	0.41	0.36	0.81	0.50	0.43
5. Bulk granulometry						
RUN5-1	0.67	1.16	1.05	0.93	1.21	1.10
RUN5-2	0.35	0.58	0.52	0.45	0.57	0.53
RUN5-3	0.33	0.45	0.42	0.37	0.44	0.43
RUN5-4	0.59	0.75	0.71	0.64	0.73	0.72
6. Particle shape						
RUN6-1	0.40	0.66	–	0.49	0.62	
RUN6-2	0.29	0.50	–	0.37	0.51	–
RUN6-3	0.23	0.41		0.31	0.44	–
RUN6-4	0.08	0.14	–	0.11	0.18	–
7. Terminal velocity model						
RUN7-1	0.16	0.42	–	0.26	0.41	–
RUN7-2	0.08	0.28	–	0.14	0.28	–

Effect of size, shape and terminal velocity on predicted ground load

Beckett F.M. et al. (2015) JGR.

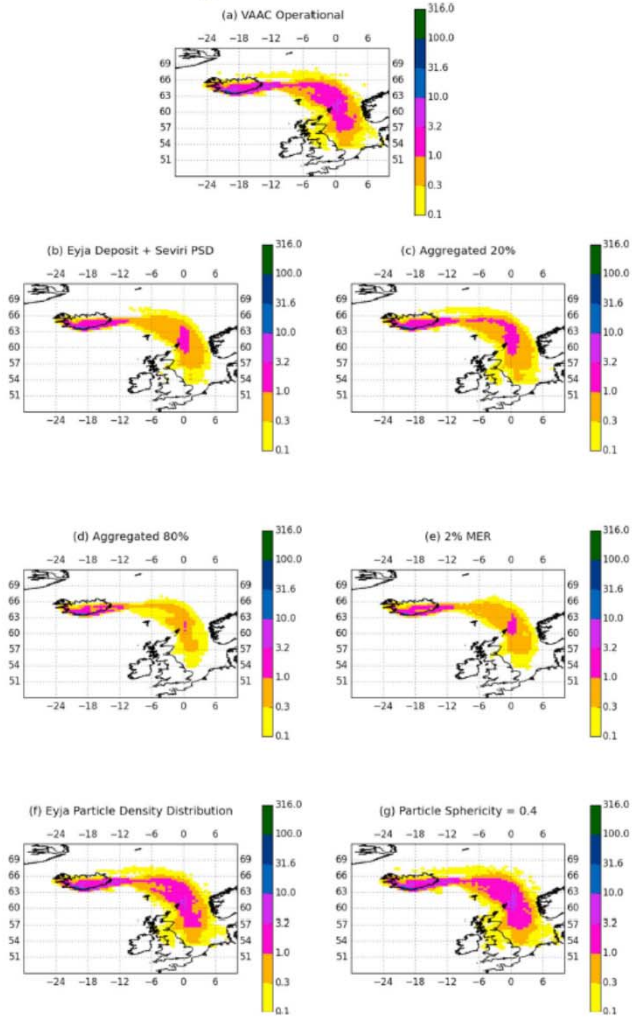

Figure 9. Comparing NAME simulated total column mass loadings (g m^{-2}) of the Eyjafjallajökull volcanic ash cloud on 17 May 2010 at 16:00 UTC. The input operational source parameters used by the London VAAC are compared to simulations where the source parameters are varied. (a and e–g) The default London VAAC PSD is used which considers particles with diameter ≤100 μm. (b–d) PSDs consider particles with diameter ≤125 μm. In all the MER applied is 5% of the total mass calculated using the Mastin relationship, except for Figure 9e where a MER of 2% is applied.

A field measurement by Taddeucci

Taddeucci J et al. (2011) Geol.

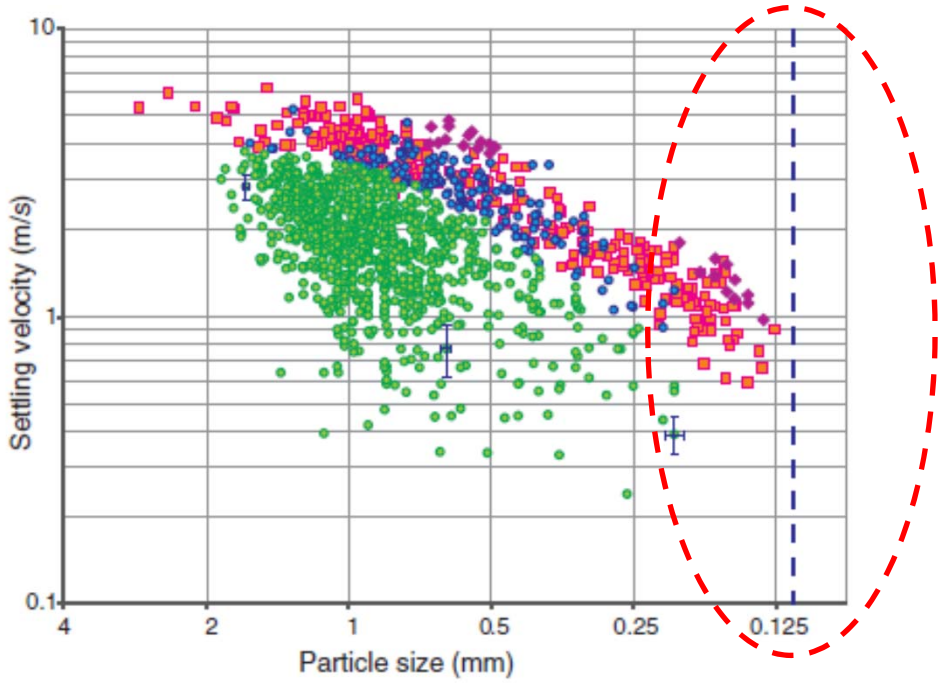

Figure 2. Size versus settling velocity of volcanic products from Eyjafjallajökull (Iceland) eruption cloud. Orange squares represent experimental data for individual ash particles. Circles represent products filmed in the field and interpreted as individual particles (blue circles) if overlapping with experimental data, or less dense aggregates (green circles) if settling at lower velocity. Purple diamonds represent test glass spheres. Note how green circles progressively thin out before disappearing at 0.2 mm, well above 0.112 mm resolution limit of recording system used in the field (blue dashed line). Error bars (±1 standard deviation) for aggregates of three different sizes are reported.

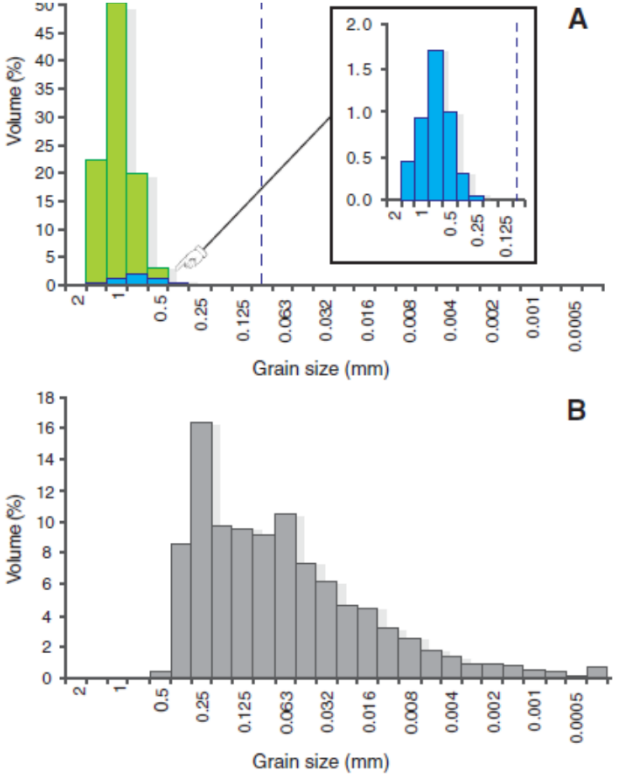

Figure 4. Grain size distribution of volcanic products from Eyjafjallajökull (Iceland) eruption. A: Aggregates (green bars) and individual particles (blue bars, enlarged in inset) as measured from high-speed video collected in the field. Size distribution is not truncated by 0.112 mm camera resolution limit (blue dashed line). Aggregates largely prevail over individual particles and show larger mode, in agreement with similar settling velocity but lower average density. B: Ash deposit collected while filming. Contribution of particles settled individually to ash deposit is negligible, and thus grain size distribution of deposit is representative of size distribution of particles settled as aggregates.

Object

Shadowgraph technique with high-intensity pulsed laser and long-distance microscope lens

Measurement of size, shape and velocity of artificial volcanic ash in the air with wide range of measurement resolution

Outline

降下火山灰の気中の運動と形状・姿勢・サイズとの同時把握を可能とする計測システムを検討した.

・シャドーイメージ法により，様々な粒子直径・真球度・沈降速度に対応可能であることを確認した.

・模擬火山灰の沈降挙動を対象に計測を行い，模擬火山灰が，非球形形状と姿勢の多様性とに起因して，沈降速度も多様性を有すること，その沈降速度の絶対値は，比重が半分程度の粒子から同程度の粒子の値に相当すること，を明らかにした.

Experimental set-up

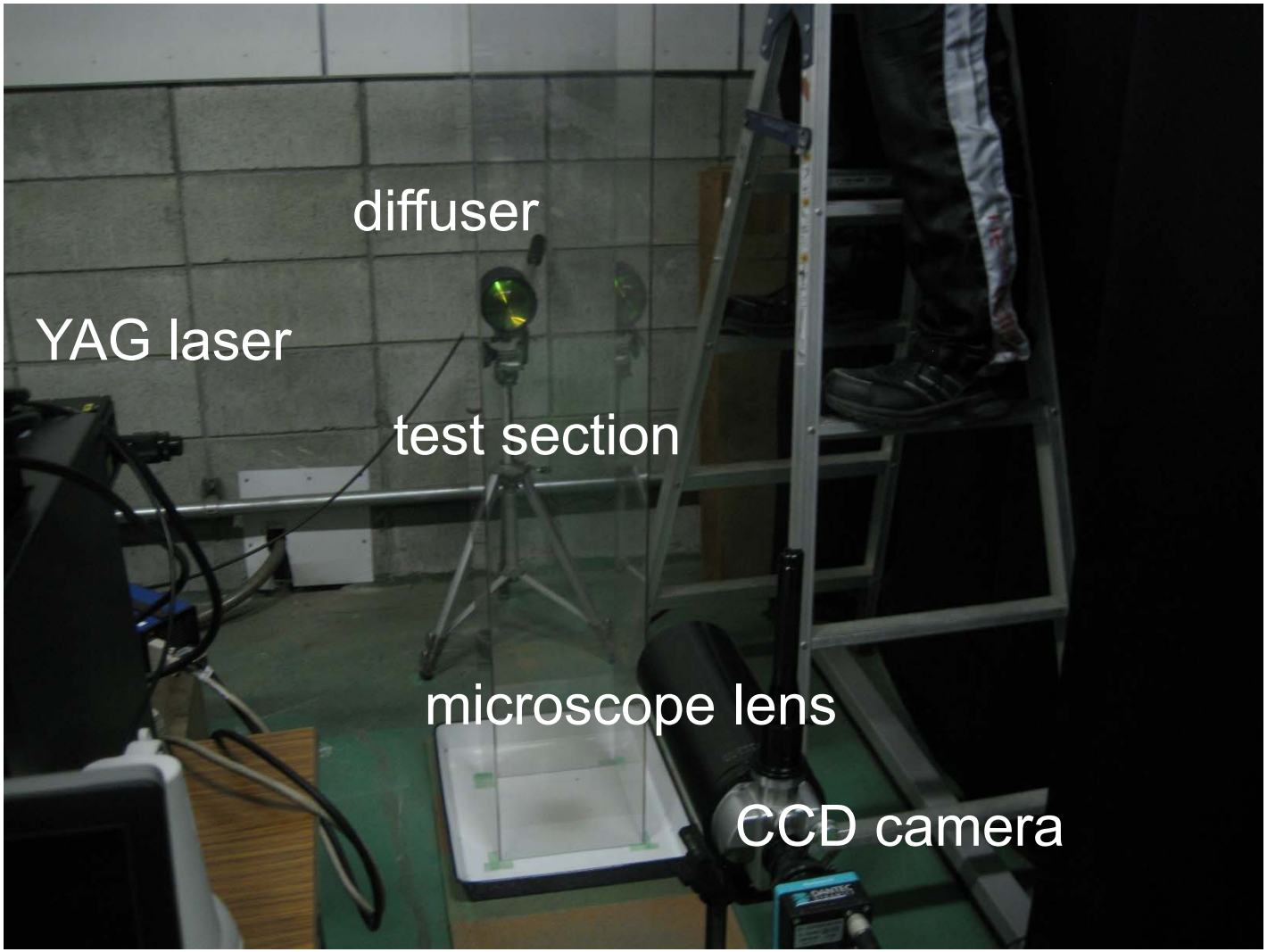

Specification of measurement system

Light source: high-intensity pulsed laser (Nd: YAG laser)

- output: 90 mJ/pulse
- wavelength: 532 nm
- attachment: diffuser lens

CCD camera:

- resolution: 4Mpixels (2014 x 2014)
- frequency: 7Hz
- attachment: long-distance microscope lens
  - Cassegrain (x125)
  - w/o, (w/) Barlow lens

Experimental condition

Measurement conditions:

- measuring location: x = 1500 mm at CL of test section
- material: ASO4 at Noga; d=75 μm and 500-2000 μm

Measurement parameters:

- pulse dt: 1000 us
- distance lens-object: 8×10^2 mm

→

physical size of visualized area: 90mm x 90 mm
physical size of CCD resolution: 0.04 mm/ pixel

Material 1

- diameter: 75 μm
- ASO4 at Noga(Takeda-shi)
- substrate of pyroclastic flow
- density: ～2300 kg m^{-3}

Material 2

- diameter: 500 – 2000 μm
- ASO4 at Noga(Takeda-shi)
- substrate of pyroclastic flow
- density: ～ 2300 kg m^{-3}

Measurement of size and shape of volcanic ash, d= 75 μm

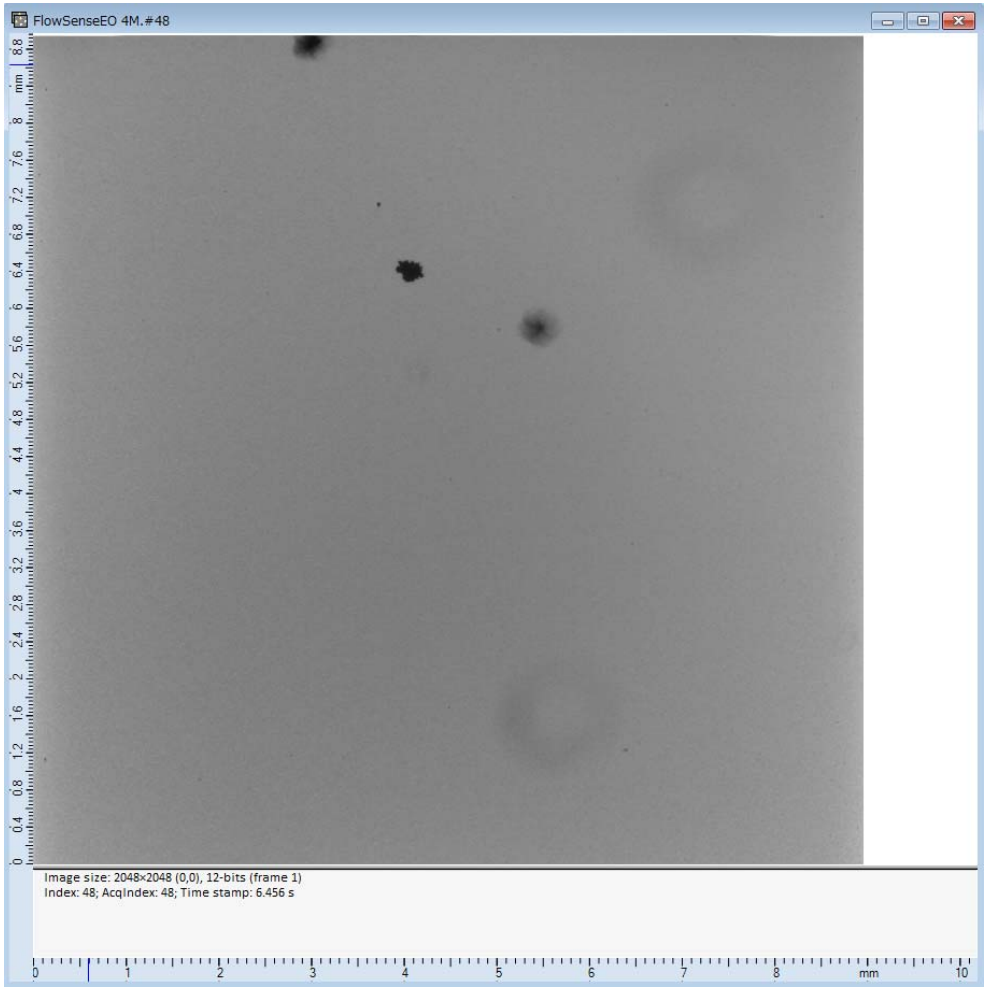

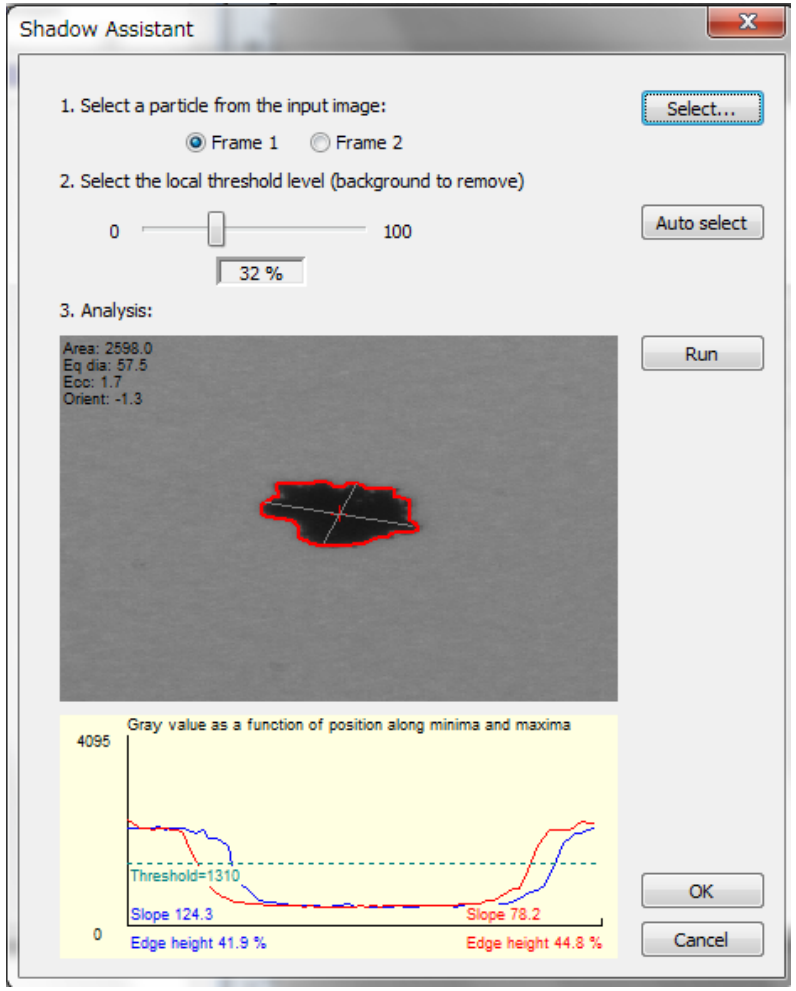

Measurement of size and shape of volcanic ash, d= 500-2000 μm

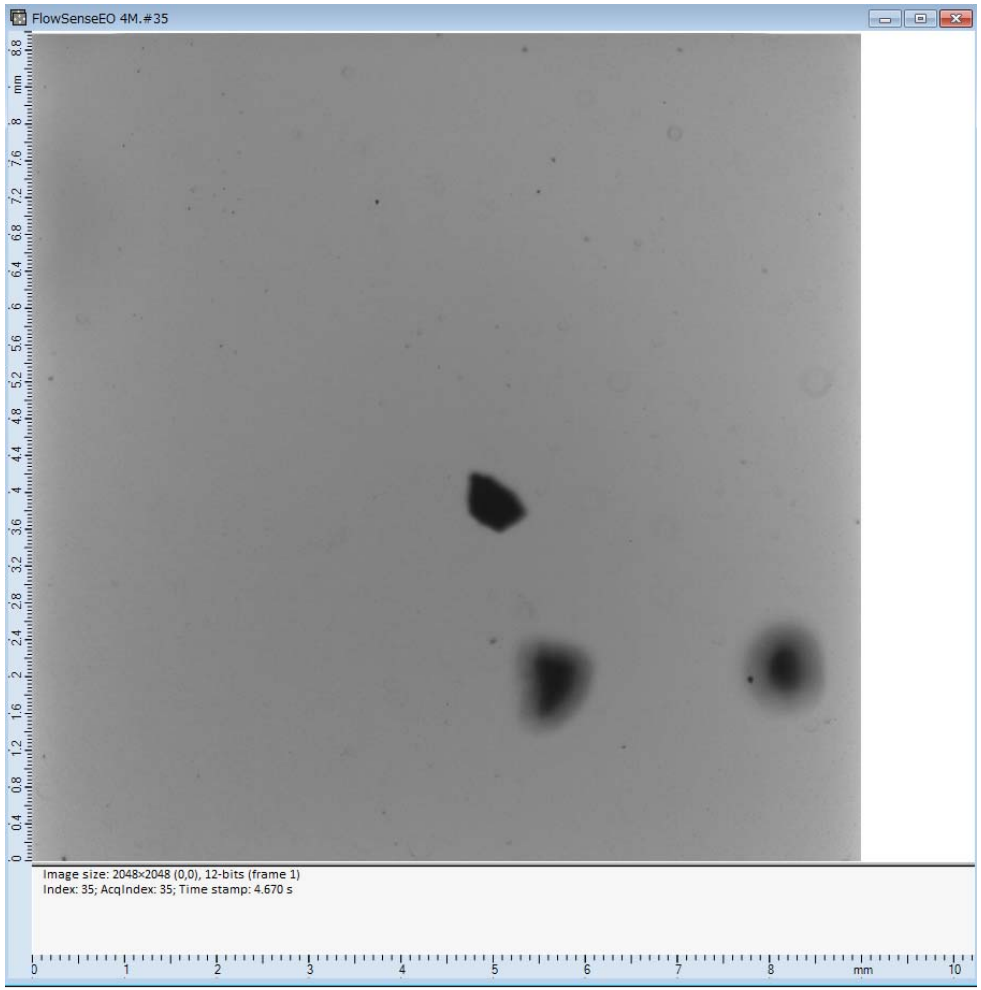

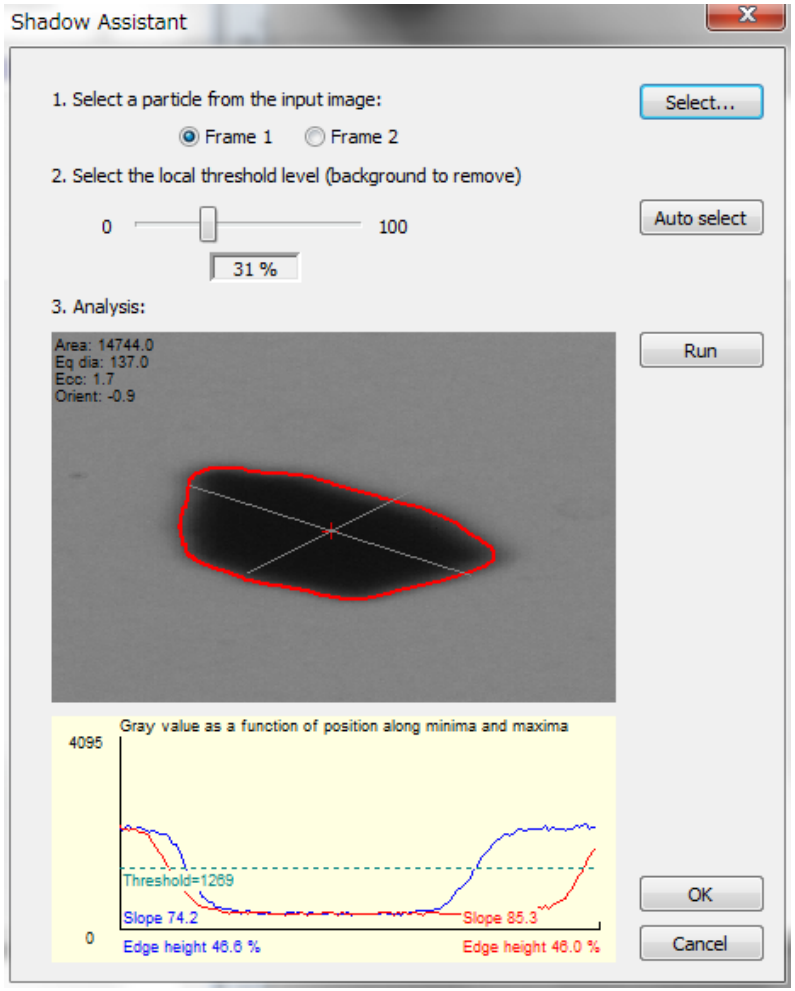

Measurement of movement of volcanic ash, d= 75 μm

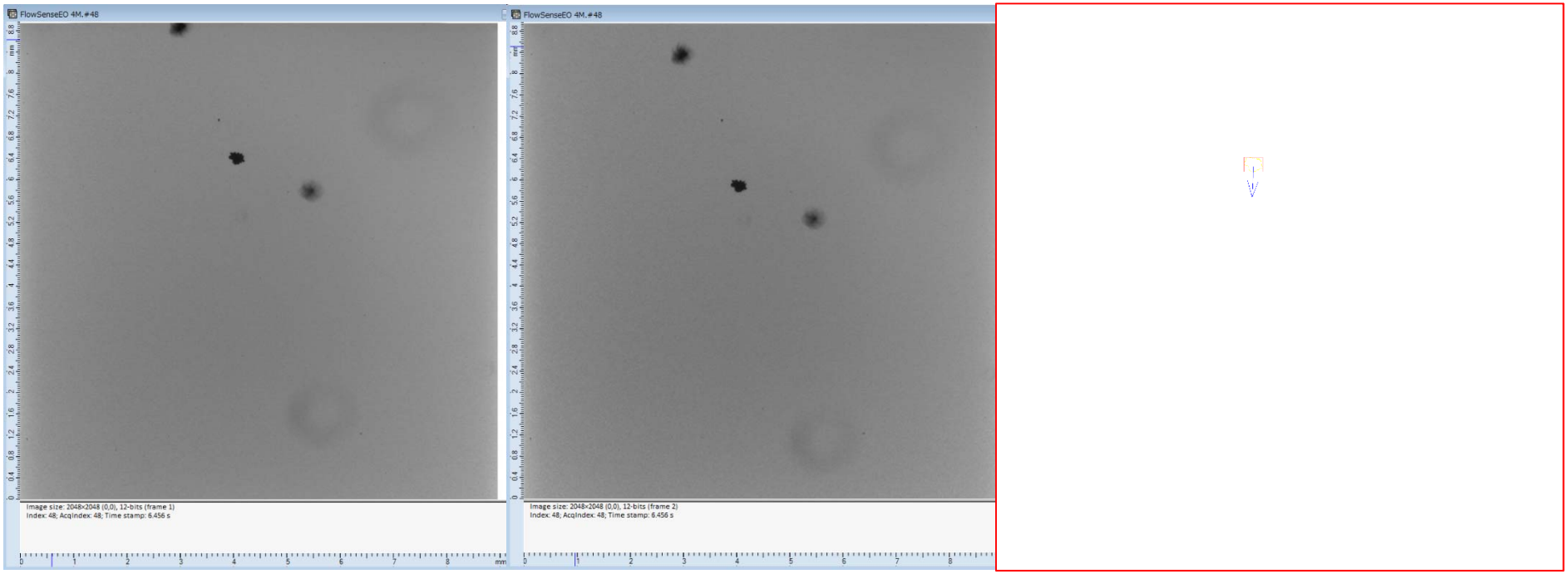

Measurement of movement of volcanic ash, d= 500-2000 μm

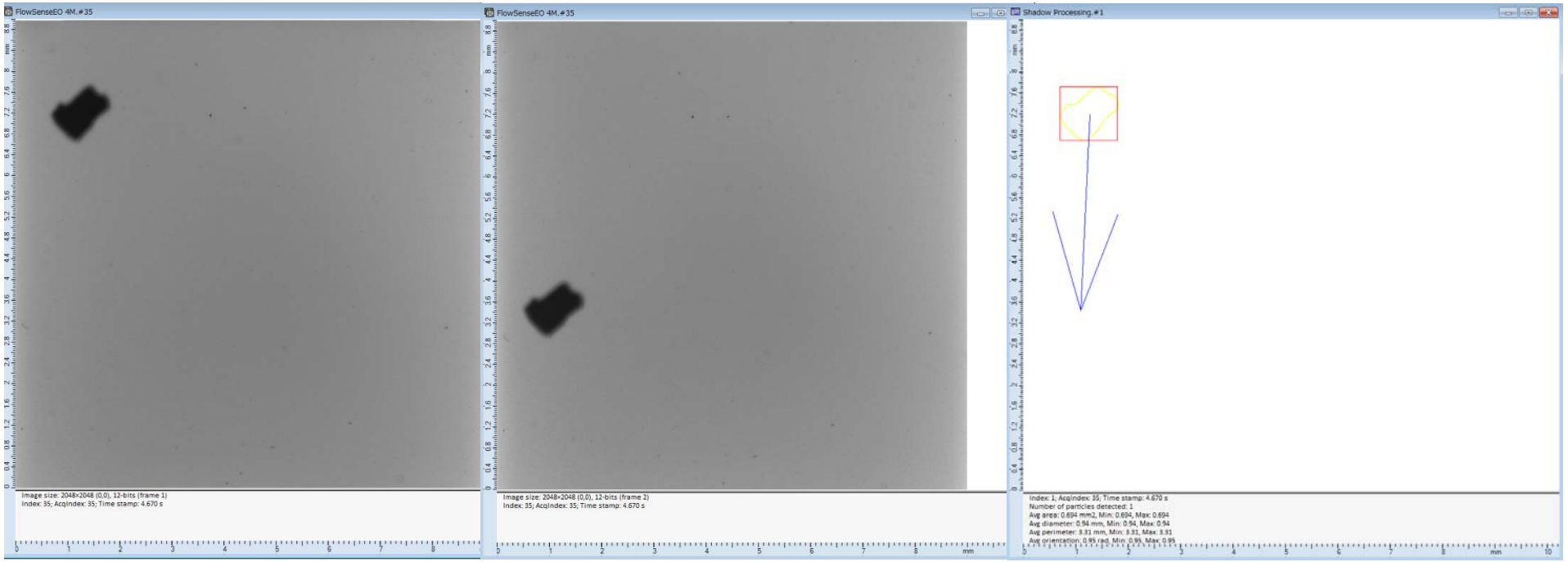

Statistics of size, shape, orientation and velocities of volcanic ash in the air

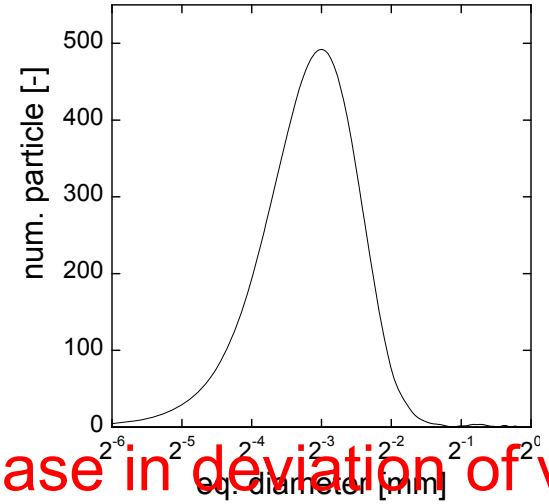

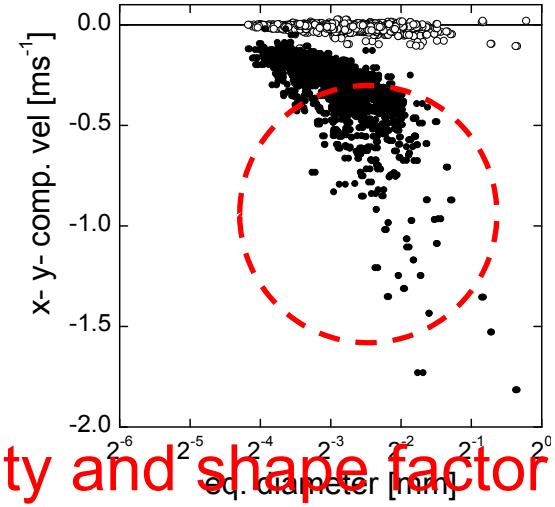

- increase in deviation of velocity and shape factor w/ d
- scattering of orientation

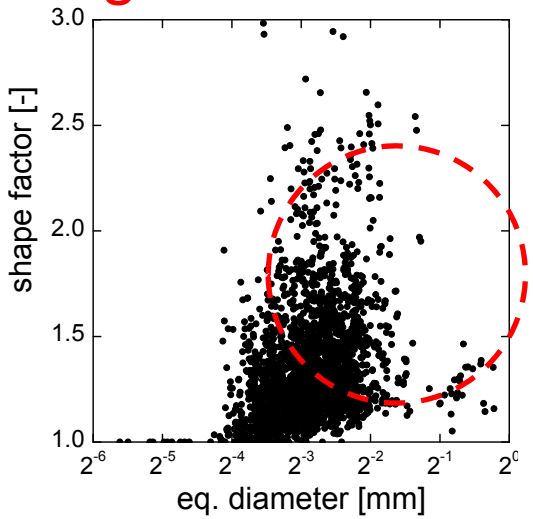

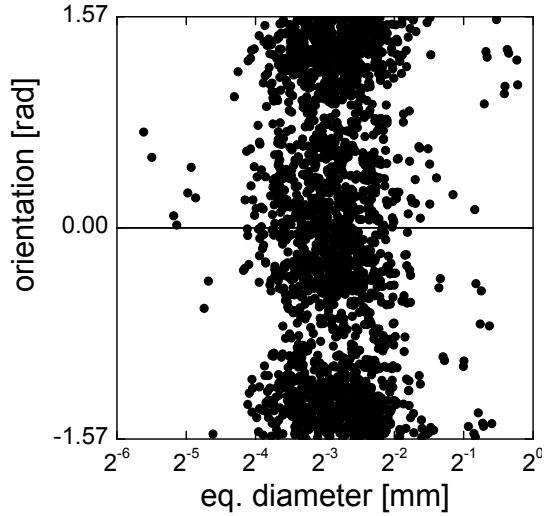

Outline

降下火山灰の気中の運動と形状・姿勢・サイズとの同時把握を可能とする計測システムを検討した.

・シャドーイメージ法により，様々な粒子直径・真球度・沈降速度に対応可能であることを確認した.

・模擬火山灰の沈降挙動を対象に計測を行い，模擬火山灰が，非球形形状と姿勢の多様性とに起因して，沈降速度も多様性を有すること，その沈降速度の絶対値は，比重が半分程度の粒子から同程度の粒子の値に相当すること，を明らかにした.

Comparison of velocities w/ sand and particles

http://www.trtc.co.jp/original.html

1. diameter
   ash: 50-2000μm
   sand: 50-200μm
   particle: 50-200μm

2. density
   ash: 2300kg m^{-3}
   sand: 2300kg m^{-3}
   particle: 1000kg m^{-3}

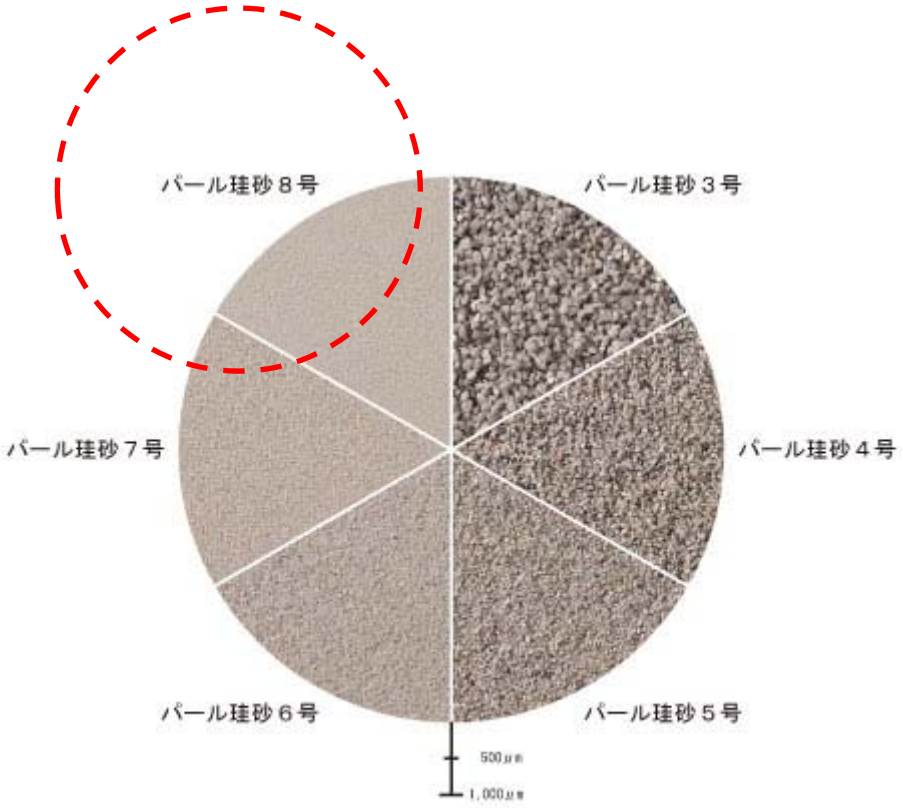

Comparison of velocities w/ sand and particles

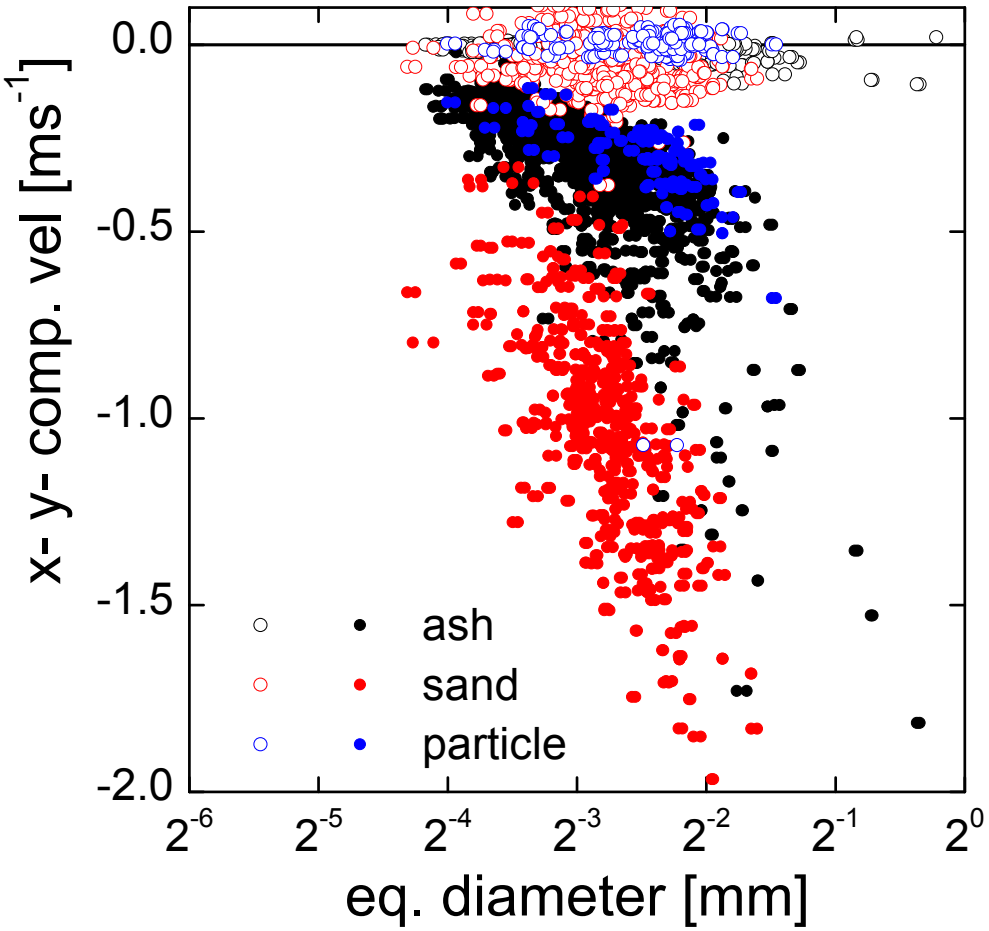

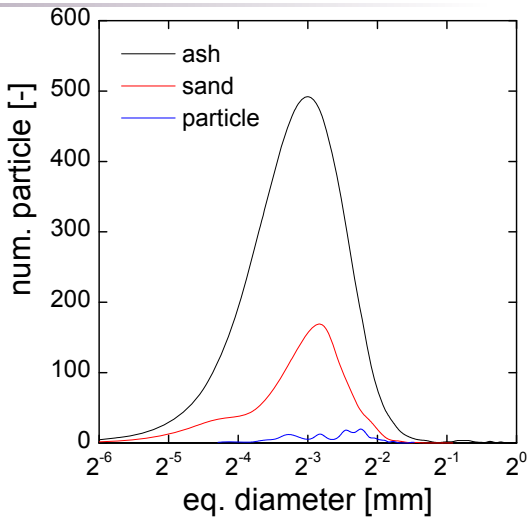

Effects of size, shape, orientation on velocities of volcanic ash in the air

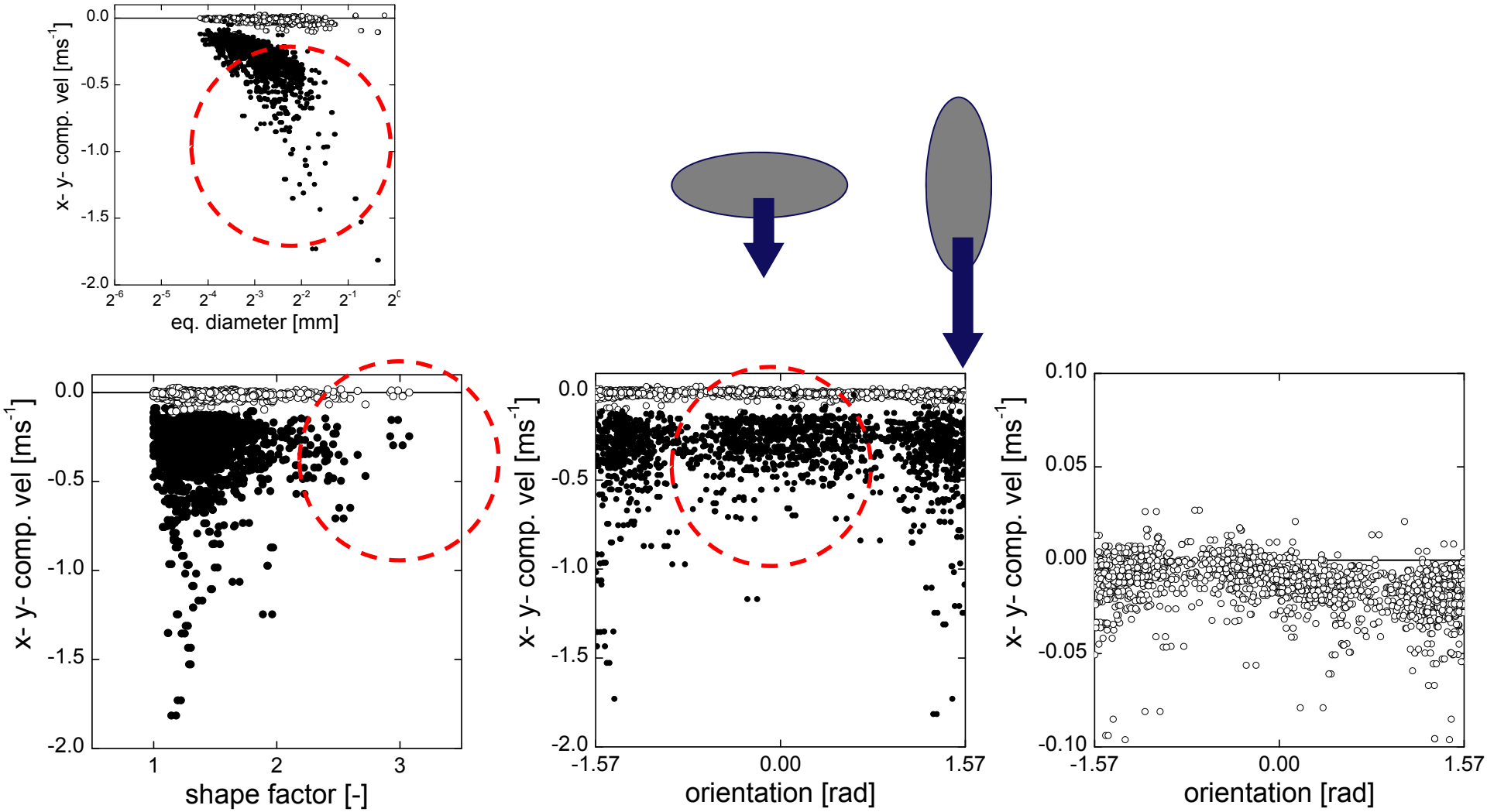

Conclusion

降下火山灰の気中の運動と形状・姿勢・サイズとの同時把握を可能とする計測システムを検討した.

・パルスレーザと長距離望遠レンズを組み合わせた光学系およびシャドーイメージ法により，様々な粒子直径・真球度・沈降速度に対応可能であることを確認した.

・模擬火山灰の沈降挙動を対象に計測を行い，模擬火山灰が，非球形形状と姿勢の多様性とに起因して，沈降速度も多様性を有すること，その沈降速度の絶対値に対して，非球形形状の影響が，比重半値の粒子に相当すること，を明らかにした.

→ 非球形粒子の形状・運動への更なる理解を進める.